



HAL
open science

The coupling of the hydrated proton to its first solvation shell

Markus Schröder, Fabien Gatti, David Lauvergnat, Hans-Dieter Meyer, Oriol Vendrell

► **To cite this version:**

Markus Schröder, Fabien Gatti, David Lauvergnat, Hans-Dieter Meyer, Oriol Vendrell. The coupling of the hydrated proton to its first solvation shell. *Nature Communications*, 2022, 13, pp.6170. 10.1038/s41467-022-33650-w . hal-03774070

HAL Id: hal-03774070

<https://hal.science/hal-03774070>

Submitted on 26 Sep 2022

HAL is a multi-disciplinary open access archive for the deposit and dissemination of scientific research documents, whether they are published or not. The documents may come from teaching and research institutions in France or abroad, or from public or private research centers.

L'archive ouverte pluridisciplinaire **HAL**, est destinée au dépôt et à la diffusion de documents scientifiques de niveau recherche, publiés ou non, émanant des établissements d'enseignement et de recherche français ou étrangers, des laboratoires publics ou privés.

17 inator structure that explains the IR spectra of both, the Zundel and Eigen cations, and
18 hence of the solvated proton? Full dimensional quantum simulations of these protonated
19 cations demonstrate that two dynamical water molecules and an excess proton constitute
20 this fundamental subunit. Embedded in the static environment of the parent Eigen cation,
21 this subunit reproduces the positions and broadenings of its main excess-proton bands.
22 In isolation, its spectrum reverts to the well-known Zundel ion. Hence, the dynamics of
23 this subunit polarized by an environment suffice to explain the spectral signatures and
24 anharmonic couplings of the solvated proton in its first solvation shell.

25 Introduction

26 The transfer of a hydrated proton between water molecules in aqueous solution is accompanied
27 by the large-scale structural reorganization of the environment as the proton relocates, giving
28 rise to the Grotthus mechanism.¹

29 Due to the complexity of the liquid phase, the infrared (IR) spectroscopy of protonated
30 water clusters in the gas phase opens a unique window to characterize and understand the elu-
31 sive structural dynamics of these species. For example, the IR spectrum of the Zundel cation
32 ($H_5O_2^+$) exhibits a prominent Fermi resonance in the $\approx 1000\text{ cm}^{-1}$ spectral region of the shared
33 proton mode due to its strong anharmonic coupling with a combination of the wagging (wa-
34 ter pyramidalization) and the oxygen-oxygen distance of the two flanking water molecules.²
35 This important feature, key to understanding the strong coupling of the shared proton to its
36 environment, could only be unambiguously measured following the development of accurate
37 messenger spectroscopy (based on Neon tagging) of the gas-phase cation.³ The theoretical
38 assignment of this feature was a computational *tour de force* only possible due to the avail-
39 ability of a high-quality potential energy surface⁴ in combination with full-dimensional (15-

40 dimensional) quantum dynamical calculations based on the multi-configuration time-dependent
41 Hartree (MCTDH) approach.^{2,5-8}

42 Recent measurements of the IR spectrum of the Eigen cation ($H_9O_4^+$) reveal a strong cou-
43 pling between the O-H stretch modes of the central hydronium unit with the water molecules
44 in its first solvation shell. More importantly, they reveal strong shifts of the spectral position of
45 the core O-H stretch modes caused by the polarization through the tagging agent in the second
46 solvation shell.⁹ The strong coupling with the first solvation shell leads to a large broadening
47 of the core O-H stretch band, now spanning about 500 cm^{-1} and markedly blue-shifted towards
48 2600 cm^{-1} in comparison with the shared proton band of the Zundel cation. The unambigu-
49 ous characterization of this very broad band has remained a long-standing challenge⁹ Yu and
50 Bowman proved that the measured spectrum in Ref. 9 can indeed be attributed to the Eigen
51 isomer. Furthermore, they showed that the broad O-H stretch feature involves multiple states of
52 the entire hydronium core¹⁰ and that in addition the O-O stretching and O-H bending motions
53 play an important role for the broadening of the O-H stretch band.^{10,11}

54 In particular, our analysis shows that the ligand waggings play an equally important role for
55 the coupling of the excess proton to its solvation shell, both in symmetrically shared Zundel
56 configurations² and in the Eigen-like form.

57 These findings were supported by detailed calculations of the linear absorption spectrum
58 of the Eigen complex with different levels of theory, most successfully using a combination of
59 QCMD and VSCF/VCI methods.¹⁰⁻¹⁴ In this paper, we simulate the linear absorption spectrum
60 of the Eigen cation for the first time using full-dimensional (33D) quantum dynamical calcula-
61 tions using polyspherical coordinates that are adapted to the Eigen motif. These allow for the
62 accurate inclusion of correlations between low frequency, large amplitude displacements and
63 the O-H stretch and other higher frequency modes. Our spectra, based on the Yu-Bowman PES
64 first published in Ref. 12 that was also applied to clusters with up to 21 water molecules,¹⁵ are

65 in excellent agreement with the available messenger-tagging spectra in the full spectral range
66 between 0 and 4000 cm^{-1} .⁹ We compare the full spectrum of the Eigen cation with those cal-
67 culated with frozen subsets of degrees of freedom all the way down to a dynamical (polarized)
68 H_5O_2^+ subunit embedded in the static scaffold of the remaining Eigen cation. This analysis
69 reveals that the underlying coupling mechanism of the solvated proton with its first solvation
70 shell is strikingly similar in both the Zundel and Eigen forms: a dynamical subunit formed by
71 two water molecules and a proton is the least common denominator structure that reproduces
72 the spectrum and anharmonic mode couplings of the Zundel and Eigen forms depending on
73 the conformation of its static environment. Along this analysis, we confirm existing assign-
74 ments^{9-13,16} of various peaks in H_9O_4^+ . We would like to stress that theoretical absorption-band
75 assignments have already been reported in Ref. 10 and are not the main focus of this contribu-
76 tion. We contribute two assignments for hitherto unknown features in the low frequency region,
77 where no experimental data is currently available.

78 **Results**

79 **IR spectrum of the Eigen cation**

80 Figure 1 shows the calculated absorption spectrum of the Eigen cation H_9O_4^+ in comparison
81 with the experimental spectra from Refs. 13 and 9. The calculated IR spectra are based on a
82 33D quantum mechanical description of the Eigen cation. Such simulations could be achieved
83 only after the unique combination of recent developments in our groups; They constitute the
84 largest quantum wavepacket simulations of a flexible molecular system using a general poten-
85 tial energy surface and curvilinear coordinates reported to date. Details of the 33-dimensional
86 quantum-dynamical calculations including the construction of the kinetic¹⁷ and potential¹⁸ en-
87 ergy operators, and the wavefunction propagations with the multilayer MCTDH method,¹⁹⁻²¹

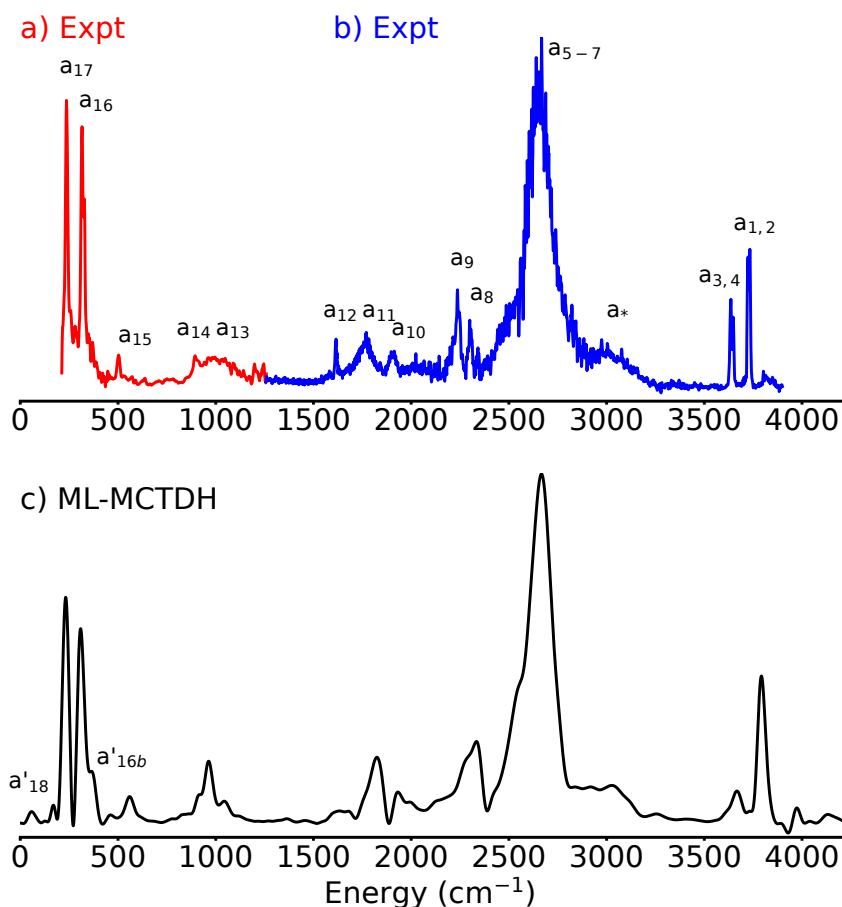


Figure 1: Absorption spectrum of the Eigen Cation H_3O_4^+ . a) Experimental spectrum from Ref. 13, b) Experimental spectrum from Ref. 9, c) Calculated spectrum (red-shifted 70 cm^{-1} to match experimental line positions). Both experimental spectra detected via photo dissociation of D_2 tagged clusters. The assignments of the peaks follow the nomenclature of Refs. 9, 13 and are discussed in Supplementary Table 1. Source data are provided under <https://doi.org/10.5281/zenodo.7064870>.

88 are provided as supporting information.

89 The calculated spectrum is red-shifted by 70 cm^{-1} to match the main features of the exper-
 90 imental spectrum. The shift originates from the fact that we obtain the ground state energy and
 91 the spectrum from separate calculations. The ground state wavefunction has a much simpler
 92 structure than the time-evolved one and it is hence better converged. This explains the global
 93 shift. The spectrum is obtained as the average over the spectra corresponding to the three po-

94 larization directions of light with respect to the molecular frame, thus considering the random
95 orientation of the molecules in the experiment (see Methods and extended data for details).

96 The overall agreement of calculated and experimental spectra is very good although the res-
97 olution of the calculated spectrum is approximately 30 cm^{-1} and limited by the 1 picosecond
98 duration of the dipole-dipole correlation function. The calculated peak positions are listed in
99 Table 1 of the supporting material alongside with experimental results and assignments. In par-
100 ticular, the substructure of the broad core O-H stretch band and practically all features of the
101 spectrum are reproduced in comparison with the tagging-agent IR measurement. Our simula-
102 tions thus further support the interpretation that (i) the spectra in Refs. 9 and 13 correspond to
103 the triply-coordinated hydronium form of $H_9O_4^+$ stoichiometry, and (ii) that the D_2 tagging-
104 agent negligibly alters the spectrum of $H_9O_4^+ \cdot D_2^{9,13}$ compared to $H_9O_4^+$.

105 **Deconstructing the broad hydronium O-H stretch band**

106 The key to understanding the anharmonic couplings of the core O-H stretch modes to their
107 first solvation shell lies in characterizing the broadening and composition of the main core O-
108 H stretch band in pristine $H_9O_4^+$: This feature carries most of the IR intensity related to the
109 coupled motions of the central proton stretching modes.

110 While studying the broad O-H stretch peak, Duong *et al.*¹¹ found that this band is char-
111 acterized by many highly entangled eigenstates in terms of normal-mode excitations. In the
112 theoretical part of their work, Duong *et al.* used VSCF/VCI calculations involving the hydro-
113 nium core modes, O-O stretch and O-H bending modes to identify states contributing to the
114 broadening. Here we take a different approach and deconstruct the formation of this band by
115 first freezing all modes of the Eigen cation, except those of the hydronium core, to their expect-
116 ation values, and then by successively bringing back the environment. The spectra obtained in
117 this way are shown in Fig. 2. They correspond to the z-component of the dipole moment (the

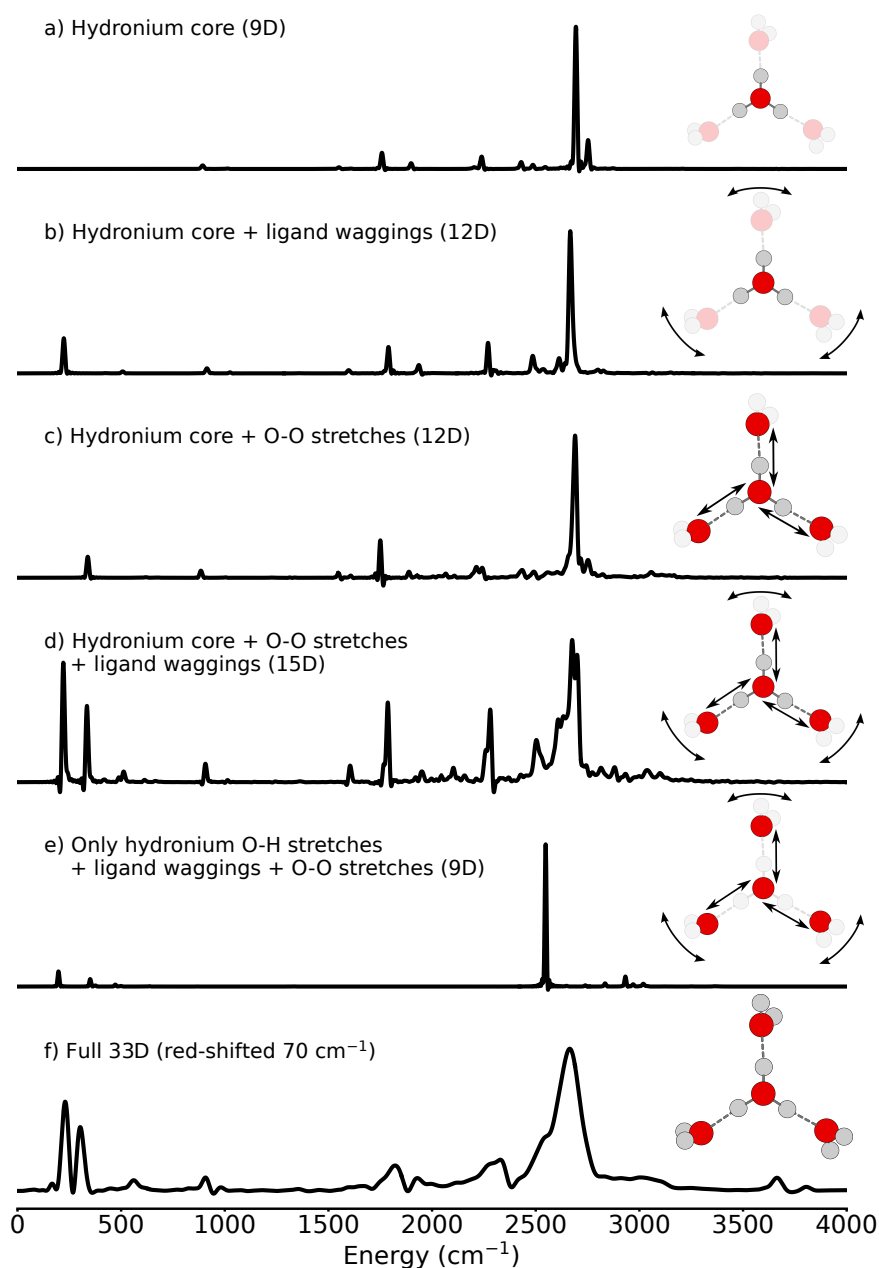


Figure 2: Spectra obtained with the z-component of the dipole moment (cf. Eq. 2) for various reduced models. The dimensionality (9D, 12D etc.) denotes the number of active coordinates. Other coordinates are frozen to their expectation value positions for the vibrational ground state. Correlation time in panels a-e): 2000 fs, panel f): 1000 fs. Source data are provided under <https://doi.org/10.5281/zenodo.7064870>.

118 polarization is aligned with one of the hydronium hydrogen bonds), since this is the component
119 responsible for the largest response of the core O-H stretchmodes. Freezing specific coordinates
120 is achieved by removing all differential operators of a frozen coordinate from the Hamiltonian
121 in a Hermitian way and by fixing their position to the corresponding expectation value in the
122 ground vibrational state of the full-dimensional system.

123 The IR spectrum of the hydronium core embedded in the frozen environment (cf. Fig. 2
124 a)) has a very simple structure. The vibrational eigenstates corresponding to the two sharp
125 peaks near 2700 cm^{-1} were obtained by full diagonalization explicitly: The dominant peak
126 corresponds to the hydronium core O-H stretch mode, whereas the smaller structure corresponds
127 to an out-of-plane excitation of the central hydrogen atoms. The peaks near 1800 and 2300 cm^{-1}
128 correspond to other modes of the hydronium core also seen in the full spectrum and agree with
129 the assignments in Refs. 9, 10, 12, 13.

130 Adding either wagging modes of the outer water molecules, Fig. 2 b), or O-O distances,
131 Fig. 2 c), leads to the appearance of their fundamental modes in the spectrum (Illustrated in
132 Fig. 3). In the latter case, some peaks on the low energy shoulder of the main O-H stretch peak
133 gain some intensity. Moreover, with the inclusion of the O-O stretching coordinates, two small
134 peaks appear at 2300 cm^{-1} correlating with a_8 and a_9 in the full dimensional spectrum. Apart
135 from this, the overall structure of the spectrum changes only slightly. In particular, there is no
136 significant broadening of the O-H stretch peak.

137 More complex spectral features emerge when adding both solvation-shell water wagging
138 modes and O-O distances together (Fig. 2 d). Now, the spectrum is not the simple sum of
139 the previous two panels and cannot be explained by the fundamental modes of the involved
140 coordinates alone. The broad hydronium core O-H stretch band centered at 2700 cm^{-1} is now
141 composed of at least four separate contributions with significant intensity. (Here we note that
142 all spectra are normalized to unity maximum height such that with the O-H stretch peak now

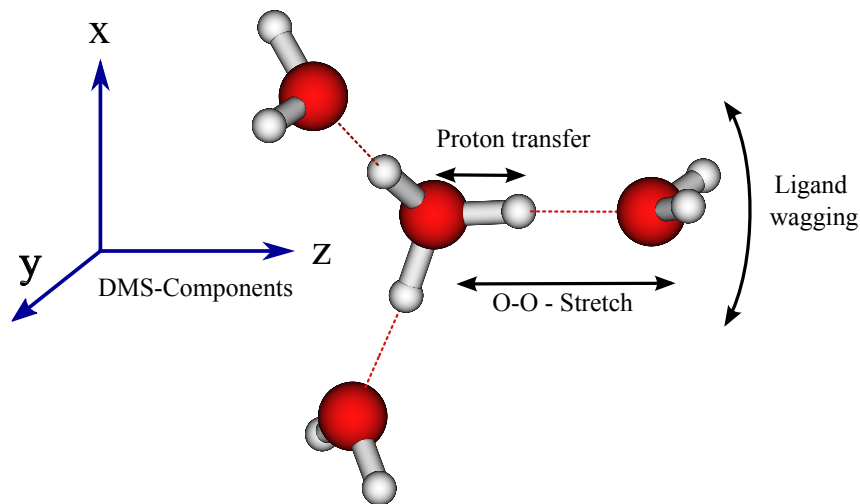


Figure 3: Illustration of ligand wagging, core O-H stretch and O-O stretching motion of H_9O_4^+ exemplary in one of the three arms of the cation. Note that in the ligand wagging motion only the two hydrogen of the outer water molecules move as indicated by the arrow. The coordinate system on the left indicates the directions of components of the dipole moment surfaces (DMS).

143 decomposing into multiple smaller peaks the relative height of all other peaks increases.) Two
 144 of those peaks, contributing to the low energy shoulder of the central peak at approximately
 145 2600 cm^{-1} , have gained significant intensity. Finally, a peak slightly above 2500 cm^{-1} gains
 146 significant intensity as well. This structure coincides with the spectral position of the low energy
 147 shoulder of the broad band in the full spectrum. Moreover, now the low intensity background on
 148 the high-energy shoulder at around 3000 cm^{-1} emerges. VSCF/VCI analysis^{11,13} attributed this
 149 to a combination mode of hydronium O-H stretch and O-O stretching modes. This assignment
 150 is fortified in Fig. 2 c) where a peak at 3000 cm^{-1} appears while only the hydronium core and
 151 the O-O stretches are modeled. Adding the ligand wagging modes then leads to the diffuse
 152 signal observed in the experimental spectrum.

153 In the spectra in panels a) to d), the hydronium core retains its full mobility. The ques-
 154 tion arises, whether only proton displacements parallel to the hydrogen bonds are important, or
 155 whether displacements perpendicular to the hydrogen bonds also contribute to the main proton-

156 transfer band. These perpendicular displacements span the hydronium bending, wagging, and
157 pyramidalization modes. Freezing the perpendicular displacements of the hydronium protons
158 (panel e)) has dramatic consequences. The spectrum is now dominated solely by the proton
159 transfer peak. Peaks of the ligand wagging and O-O stretching fundamentals are again visible
160 with low intensity at low energies, as well as peaks at approximately 3000 cm^{-1} that are com-
161 binations of hydronium core O-H stretch, ligand wagging, and O-O stretch modes. However,
162 the inability of the three central protons to move perpendicular to the hydrogen bond directions
163 has largely suppressed their coupling with the first shell of ligand water molecules. Crucially,
164 no broadening of the O-H stretch peak is present, as opposed to the spectrum in panel d). This
165 leads to the conclusion that the vibrational eigenstates spanning the broad hydronium core O-H
166 stretch band correspond to combinations and overtones of the central O-H stretch modes with
167 O-O stretch displacements, hydronium bending and hydronium wagging, and ligand waggings,
168 whereby none of those coupled hydronium and environment modes can be removed. A full
169 characterization of the vibrational eigenstates in terms of quantum numbers of some basis of
170 uncoupled vibrational modes is currently out of reach due to the very high density of vibrational
171 states in the spectral region of the band and the high dimensionality of the problem.

172 **The dynamical H_5O_2^+ subsystem**

173 We have deconstructed the main hydronium O-H stretch band. It originates from the anhar-
174 monic couplings of the center O-H stretch modes with perpendicular modes of the central hy-
175 dronium and modes involving the O-O stretchings and waggings of the three surrounding water
176 ligands. The question now arises: Are the three water molecules in the first solvation shell of
177 the Eigen cation necessarily involved in explaining the coupling mechanism, spectral position,
178 and width of the main proton-transfer band? Alternatively, can a smaller dynamical subunit
179 completely account for the properties of the first solvation shell of the solvated proton? The

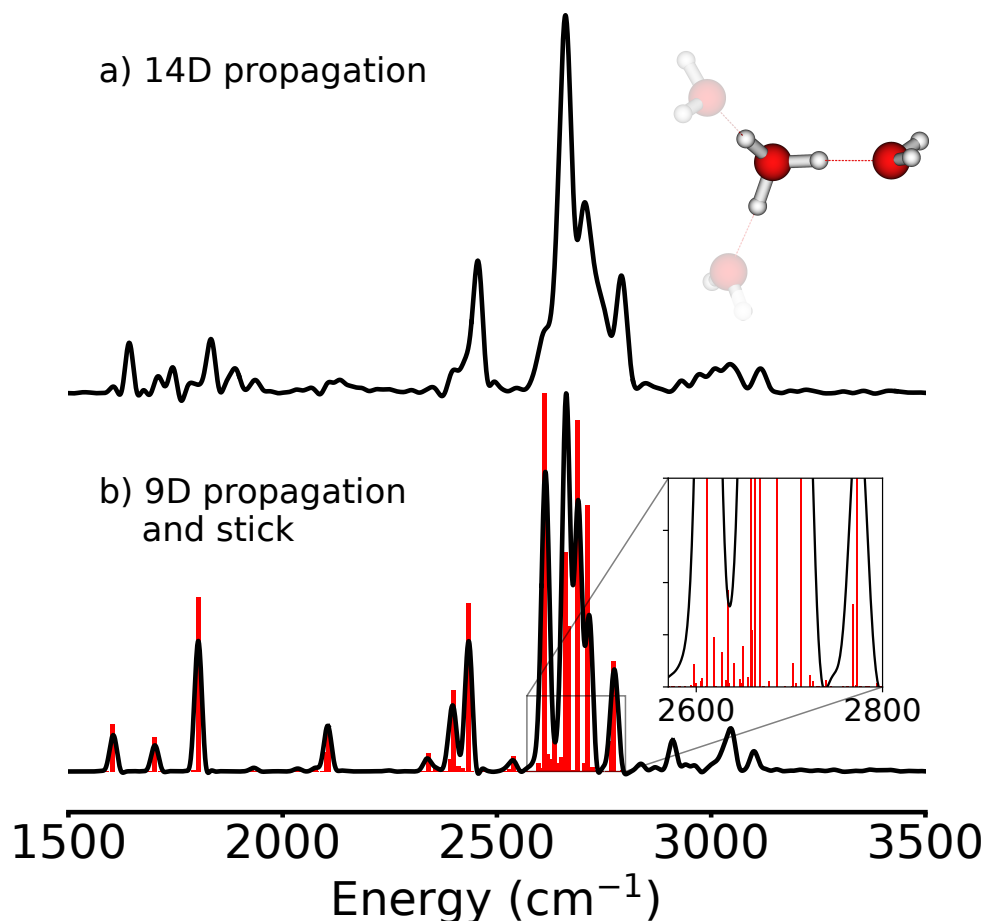


Figure 4: Spectra obtained with the z-component of the dipole moment surfaces for a reduced H_5O_2^+ model obtained by freezing modes to positions corresponding to their expectation values for H_9O_4^+ a) obtained with a dipole-dipole-correlation function of 2000 fs using a 14D model, b) obtained with a dipole-dipole-correlation function of 2000 fs using a 9D model (black curve), and obtained as a stick spectrum using eigenstates (red lines). Source data are provided under <https://doi.org/10.5281/zenodo.7064870>.

180 hydronium cation (H_3O^+) can be discarded as the least common denominator subunit by com-
 181 paring Figs. 2 a) and f). Even though the O-H stretch peak in Fig. 2 a) is in the correct position,
 182 broadening is not observed.

183 Instead, we consider one H_5O_2^+ subunit, that can be understood as a polarized Zundel cation
 184 (14 coordinates) and freeze all internal, angular and relative coordinates of the two other wa-
 185 ter ligands to their corresponding expectation values positions (cf. Fig. 4), as well as the two

186 free-standing hydronium O-H stretches, as those do not interact with their immediate envi-
187 ronment dynamically any more. For comparison, we also consider a reduced version of the
188 H_5O_2^+ @Eigen cation where the rocking, relative water rotation and internal modes of the ex-
189 ternal water are also frozen, thus yielding a 9-dimensional system for which the lowest 250
190 eigenstates can be computed with the improved relaxation algorithm (ticks in Fig. 4b)).^{22,23}

191 The IR spectrum of the dynamical H_5O_2^+ @Eigen cation is strikingly similar to the full Eigen
192 cation spectrum, as seen in Fig. 1. The main O-H stretch band presents a comparable broadening
193 and is centered at the same frequency. Other flanking peaks appear at the correct positions as
194 well. The analysis of 1D and 2D probability densities of the calculated eigenstates of the 9-
195 dimensional model reveal that the vibrational states that participate in this band are complex
196 combinations and overtones of the same vibrational coordinates previously found to contribute
197 to the broadening of the core O-H stretch band in the Eigen cation. Just pulling the external
198 water molecules by about 0.5 Å away from the central hydronium, while leaving them frozen,
199 results in a shift of the O-H stretch band to the red by about 600 cm^{-1} (cf. supporting material)
200 as well as a reduction of the ground state expectation value of the O-O distance by 0.1 Å and an
201 increase of the O-H distance expectation value by 0.06 Å. This indicates the extreme sensitivity
202 of the position of this band to the polarization by the first solvation shell of water molecules.
203 This trend has also been observed in similar studies on protonated water clusters.²⁴⁻²⁸ Pulling
204 the waters further to infinity leaves the bare Zundel cation with its O-H stretch band red-shifted
205 by about 1600 cm^{-1} compared to the Eigen cation.²

206 Based on these observations, we argue that *two* protonated water molecules, nominally the
207 polarized H_5O_2^+ /Zundel subunit, constitute the *dynamical* least common denominator structure
208 explaining the anharmonic couplings and spectral signatures of the solvated proton in its first
209 solvation shell. This statement does not concern the relative population of the Zundel and Eigen
210 structures in solution, which has been investigated separately by Marx and collaborators using

211 path integral techniques, cf. Ref. 1.

212 In isolation, the main shared-proton peaks in the Zundel cation are strongly red-shifted com-
213 pared to the Eigen cation. The shared-proton motion strongly couples to the wagging (pyrami-
214 dalization) of the two water molecules and to the O-O stretching mode, and results in the well-
215 characterized Fermi resonance doublet centered at about 1000 cm^{-1} .^{5,6,29,30} Embedded in the
216 potential of two flanking, frozen water molecules, the polarized H_5O_2^+ @Eigen subsystem fea-
217 tures its O-H stretch band at the same spectral position as the full-dimensional Eigen cation, i.e.
218 blue-shifted to about 2600 cm^{-1} because the shared proton is now much closer to the central wa-
219 ter molecule. The broadening of the core O-H stretch band in the polarized H_5O_2^+ @Eigen and
220 Eigen cations is strikingly similar. Our simulations demonstrate that the same set of vibrational
221 coordinates and corresponding combined excitations are responsible for the strong coupling of
222 the shared proton to the rest of the scaffold in the Zundel,^{5,6,29,30} polarized H_5O_2^+ @Eigen and
223 Eigen cations. These effects are strongly cooperative as opposed to additive. These relevant
224 coordinates are the hydronium O-H bending and wagging modes, the ligand water wagging
225 modes, and the O-O hydrogen bond stretching mode.

226 Discussion

227 This work has provided a set of full-dimensional quantum simulations of the Eigen cation based
228 on flexible, curvilinear coordinates and a very accurate potential energy representation. The
229 simulated IR spectra cover the chemically relevant spectral range between 0 and 4000 cm^{-1}
230 with one single time-propagation of a highly correlated multiconfigurational wave function.
231 The spectra extend below the smallest frequency accessible experimentally using ion tagging
232 techniques, and reveal the signatures of very low frequency, global vibrational modes. Both the
233 Zundel and Eigen cations feature very prominent spectral features related to the anharmonic

234 couplings of the hydrated proton with its first solvation shell. In the Zundel cation, a strongly
235 red-shifted double peak^{6,30} originates from the fundamental vibration of the equally shared pro-
236 ton at about 1000 cm^{-1} . This doublet is a Fermi resonance that involves the wagging modes
237 of the flanking water molecules as well as the hydrogen-bond O-O stretching. The isolated
238 Eigen cation, instead, features a very broad band at 2600 cm^{-1} with little resemblance to the
239 shape and position of the Zundel's double peak. Nonetheless, a careful analysis reveals that
240 similar anharmonic couplings compared to the Zundel form are involved in the broad Eigen
241 cation band, namely the hydronium and ligand waggings to the largest extent, combined with
242 hydrogen-bond stretchings. Indeed, the hydronium waggings are crucial to the coupling mech-
243 anism: freezing the central hydronium waggings in a flexible first solvation shell results in a
244 simpler IR spectrum than when considering a fully flexible hydronium in a frozen environment
245 (cf. Figs. 2a and e).

246 Based on these results and observations, we arrive at a key insight: two dynamical water
247 molecules and a proton, i.e. a H_5O_2^+ subunit embedded in the remaining frozen scaffold of
248 the Eigen cation, presents all anharmonic couplings and spectral signatures of the fully flexible
249 Eigen cation in the region of the main proton-transfer band. Depending on its environment, the
250 H_5O_2^+ subunit can describe both the spectrum of the Zundel and Eigen cations. For this effect,
251 it is sufficient that two frozen, hydrogen-bond acceptor water molecules polarize the dynamical
252 H_5O_2^+ subunit that constitutes the proton's first solvation shell. This finding, backed by our full
253 quantum-mechanical approach, is suggestive of picturing the Eigen cation as three overlapping
254 and strongly polarized H_5O_2^+ subunits in the spirit of the classical 'special pair dance' models
255 of the solvated proton.³¹⁻³³

256 The question of whether the proton forms an Eigen or Zundel cation in aqueous acid so-
257 lutions has given rise to many studies even recently: some new experimental works³⁴⁻³⁶ have
258 suggested that the population of the Zundel cation is larger than previously thought. On the

259 other hand, new simulations³³ have interpreted these experimental findings in an opposing sense
260 pointing to a dynamic Eigen cation as the most prevalent hydrated proton species. Our new re-
261 sults do not bring information about the relative populations of the two structures, but stress
262 that the difficulty to solve the problem may partly come from the fact that the H_5O_2^+ subunit
263 can exhibit very similar spectral signatures compared to the Eigen cation when placed in a
264 polarizing environment. Establishing these structural and dynamical relations on the basis of
265 full-dimensional quantum dynamics is an important direction for future work. The computa-
266 tional and theoretical developments reported in this work may be decisive when approaching
267 even larger and more complex systems.

268 **Methods**

269 **High-dimensional quantum dynamics**

270 The full-dimensional (33 vibrational degrees of freedom) quantum dynamical description of the
271 IR spectrum of the Eigen cation requires the combination of various technologies that have been
272 developed and integrated into the software packages maintained in our research groups. These
273 technologies relate to the three main obstacles that stand on the way towards a full quantum
274 dynamical description of anharmonically coupled, flexible, and high-dimensional vibrational
275 problems.

276 (i) Describing flexible and anharmonic systems, e.g. with several equivalent minima in their
277 potential energy surface (PES), requires the use of chemically meaningful coordinates such as
278 bond lengths, bond angles, and dihedral angles. The use of adequate coordinates enormously
279 facilitates the numerical representation and convergence of the vibrational wavefunctions in
280 high-dimensions. The price to pay, though, is the very lengthy and complicated expression for
281 the corresponding kinetic energy operator (KEO). For the Eigen cation, the exact, analytic KEO

282 has a total of 4370 terms and its manual derivation becomes *de facto* intractable. Some of us and
283 others have therefore developed a completely systematic method to set up the KEO for a spe-
284 cific family of internal molecular coordinates: the polyspherical coordinates.³⁷⁻³⁹ This method
285 is implemented in the TANA software, which provides analytic expressions of the kinetic energy
286 operator in a machine readable format^{17,40,41} Very importantly, TANA also provides numeri-
287 cal library routines to perform forward and backward transformations between the Cartesian
288 coordinates of the atoms and the internal coordinates of the molecule, which are needed when
289 setting up the potential energy operator in these internal coordinates.

290 (ii) The second obstacle is the so-called “curse of dimensionality” for representing and stor-
291 ing the wavefunction of the system: the number of possible quantum states of the system (e.g.
292 given as the amplitudes on quadrature points in coordinate representation) grows exponentially
293 with the number of physical coordinates. Without an efficient data reduction scheme one would
294 be limited to model up to about six internal degrees of freedom of a molecule, correspond-
295 ing to about four atoms (neglecting rotations). To overcome the curse of dimensionality, the
296 state vector needs to be stored and processed in a very compact form. To this end, we em-
297 ploy the multi-layer multi-configuration time-dependent Hartree algorithm,^{19-21,42,43} which rep-
298 resents the wavefunction as a hierarchical Tucker tensor-tree.⁴⁴⁻⁴⁶

299 (iii) The solution of the time-dependent Schrödinger equation within this tensor format re-
300 quires that also the system Hamiltonian is expressed in a matching form. This can be, e.g., a
301 sum of products of low-dimensional operators. The KEO in polyspherical coordinates always
302 consists of sums of products of elementary functions and derivatives of single coordinates³⁹
303 (this is one of the main advantages of the polyspherical coordinates) and needs not be discussed
304 further here. A more challenging task is to express the PES and, if needed, other surface-like
305 operators such as dipole moment surfaces (DMS), in a matching format. The PES and DMS
306 are usually made available as separate software libraries, and are often defined in the Cartesian

307 coordinates of the atoms.^{10,12,16} Most applications in our groups have relied until recently on
308 the transformation of the PES into a Tucker format with the so-called Potfit algorithm,⁴⁷⁻⁴⁹ and
309 its hierarchical multi-layer variant.⁵⁰ This algorithm suffers from the curse of dimensionality
310 because ultimately it requires a full representation of the primitive product grid in configuration
311 space. Modifications of Potfit have been developed over the years to partially overcome this
312 difficulty,⁵¹⁻⁵³ making it possible to work with about 9 to 15 coordinates. This is clearly insuf-
313 ficient to approach a system of the size of the Eigen cation. A more recent development in sur-
314 face re-fitting uses the so-called canonical tensor decomposition⁵⁴ (CP), also called PARAFAC
315 or CANDECOMP in the literature.^{55,56} Within the canonical format, orthogonality restrictions
316 on the basis functions are relaxed such that a much more compact tensor representation can be
317 achieved, at the cost however, that the fit is much harder to obtain. This is usually achieved us-
318 ing an alternating least squares (ALS) algorithm that iteratively improves an initial guess tensor.
319 The ALS algorithm in the original form requires to perform high-dimensional integrals as well.
320 In a recent publication¹⁸ Monte-Carlo integrations are used to perform the integrals. This not
321 only mitigates the curse of dimensionality but also allows for importance sampling such that
322 low energy regions of the potential (where the wavefunction resides) can be fitted with elevated
323 accuracy. This development has opened the path to obtain global but compact surface fits in a
324 tensor format of high-dimensional potentials.

325 In essence, we developed and combined three technologies to be able tackle such a high-
326 dimensional problem as the 33-dimensional Eigen cation: 1) the TANA software to obtain the
327 KEO and to provide the coordinate transformations for the PES fitting; 2) PES fitting into a
328 canonical tensor format using a Monte-Carlo version of the ALS algorithm; and 3) the multi-
329 layer MCTDH algorithm to solve the time-dependent Schrödinger equation. In the present
330 contribution we have used the highly accurate, full-dimensional PES and DMS provided by Yu
331 and Bowman.^{10,12,16} The surfaces were re-fitted into a canonical tensor format using 2048 terms

332 for the PES and 1024 terms for each of the three components of the DMS, respectively.

333 **Calculation of IR Spectra**

334 The linear absorption spectra that are compared to the experimental spectra are computed as
335 averages of the spectra resulting from the three dipole moment components for the x - y - and
336 z -directions as

$$I(\omega) = \frac{1}{3}(I_x(\omega) + I_y(\omega) + I_z(\omega)). \quad (1)$$

337 The averaging mimics the random orientational distribution of the molecule in the experiment.

338 The single components also shown in some figures below are calculated as⁶

$$I_j(\omega) \propto \omega \operatorname{Re} \int_0^{\infty} dt \langle \Psi_{\mu_j} | \Psi_{\mu_j}(t) \rangle \exp(i(\omega + E_0/\hbar)t), \quad j = x, y, z \quad (2)$$

339 where E_0 is the ground state energy and

$$|\Psi_{\mu_j}\rangle = \mu_j |\Psi_0\rangle \quad j = x, y, z \quad (3)$$

340 is the vibrational ground state $|\Psi_0\rangle$ operated with μ_j , one component of the dipole operator. The
341 time-dependent state $|\Psi_{\mu_j}(t)\rangle$ is obtained by solving the time-dependent Schrödinger equation
342 with initial value $|\Psi_{\mu_j}\rangle$.

343 **Assignments**

344 To assign modes to the peaks a number of test states that contain zero order excitations in
345 selected modes have been created and cross-correlated with the dipole operated and propagated
346 ground state.

347 The Fourier transform of the resulting cross correlation shows peaks only at frequencies

348 where both, the test states and dipole operated ground states populate the same eigenstate. The
 349 cross-correlation-functions are defined as

$$C_{i,X}(t) = \langle \Psi_X | \Psi_{\mu_i}(t) \rangle \quad i = x, y, z \quad (4)$$

350 and $|\Psi_X\rangle = X |\Psi_0\rangle$ being the X -operated ground state with an operator X as detailed below.
 351 The Fourier transformed of the cross-correlation is given as

$$F_{i,X}(\omega) = \propto \text{Re} \int_0^{\infty} dt \langle \Psi_X | \Psi_{\mu_i}(t) \rangle e^{i(\omega + E_0/\hbar)t} \quad i = x, y, z, \quad (5)$$

352 with E_0 being the ground state energy. Note that, other than for the absorption spectra, no
 353 frequency prefactor ω is multiplied to the spectrum.

354 The test-states $|\Psi_X\rangle = X |\Psi_0\rangle$ have been created by constructing the operator X as linear
 355 combinations of position operators of specific coordinates. This creates a linear combination
 356 of wavefunctions, with nodes in the respective modes, hence resembling zero order excitations
 357 which mimic the action of the dipole moment surface but restrict the action only to the afore-
 358 mentioned modes. We use the notation $q(+++)$, $q(-++)$ and $q(0-+)$ for X in the test
 359 states. Here the q indicate physical coordinates and the string of signs in brackets identifies one
 360 of the three orthogonal linear combinations of the coordinates q in the three 'arms' A, B, and C
 361 of the Eigen cation (cf. Fig. S8, extended data), where specifically

$$q(+++) := q_A + q_B + q_C \quad (6)$$

$$q(-++) := -2q_A + q_B + q_C \quad (7)$$

$$q(0-+) := -q_B + q_C \quad (8)$$

362 (with the exception of label $q = \theta' = (q_A = \theta, q_B = \varphi_{AB}, q_C = \varphi_{BC})$, and $q = \mathbf{b}'$ describing the

363 ligand O-H bending as a linear combination of two Jacobi coordinates $b_{\{A,B,C\}} = -0.4 r_{1,\{A,B,C\}}$
 364 $+ 0.3 r_{2,\{A,B,C\}}$. Similarly the symmetric O-H stretching of the ligands is described by $q = v^{(s)}$,
 365 with $v_{\{A,B,C\}}^{(s)} = 0.3 r_{1,\{A,B,C\}} + 0.4 r_{2,\{A,B,C\}}$, while the asymmetric O-H stretching $v_{\{A,B,C\}}^{(a)} =$
 366 $\nu_{\{A,B,C\}}$ is described by the Jacobi angle., cf. Table S1 of assignments and Table S2 and Fig. S9
 367 of coordinate definitions in the extended data section).

368 Non-vanishing cross-correlations hence show the existence of non-vanishing overlap of the
 369 dipole operated state Ψ_{μ_i} and the test state characterized by a linear combination of single mode
 370 excitations of character Eq. (7).

371 **Kinetic energy operator**

372 As for the Zundel cation,²⁹ we adopted a mixture of Jacobi, Cartesian, and valence vectors. For
 373 each external molecule of water (in blue in Fig. S7, extended data), we use two Jacobi vectors:
 374 one from one hydrogen atom to the other and one from the middle of H₂ to the oxygen atom.
 375 The central oxygen atom is linked to the other oxygen atoms by three O-O valence vectors.
 376 The global z Body-Fixed (BF) axis is parallel to R_1^{BF} , one of the O-O vectors. The groups S^1
 377 and S^2 are gathered into two subsystems so that they have their own BF frame with the z axis
 378 parallel to R_2^{BF} or R_3^{BF} . The molecule at the top of Fig. S7 (extended data) is also gathered
 379 in one subsystem with the z axis parallel to the H-H vector. The same is true for the other two
 380 molecules of water except that they define "subsubsystems" in S^1 and S^2 . The three OH valence
 381 coordinates starting from the central oxygen atom are re-expressed in terms of Cartesian (and
 382 not spherical) coordinates to avoid singularities in the kinetic energy operator (KEO).

383 All the other vectors are parametrized by spherical coordinates in their BF frame. The rota-
 384 tion of each BF frame is parametrized by Euler angles. We follow the conventions of the general
 385 formulation for polyspherical coordinates⁵⁷ that is implemented in the TANA software^{17,40} The
 386 correctness of the implementation has been checked on many systems by comparing the KEOs

387 with those obtained numerically with the TNUM software.^{41,58} We thus obtain an exact oper-
388 ator. TANA provides the operator in an ascii file that can be directly read by MCTDH. One
389 advantage of the family of polyspherical coordinates is that it always leads to an operator in a
390 sum of products of one-dimensional operators. In the present case, with those coordinates and
391 their corresponding ranges, we avoid all the possible singularities in the KEO so that we do not
392 need to use 2D DVRs that are numerically less efficient than products of 1D DVRs.

393 **Sum-of-products of potential and dipole moment surfaces**

394 In the present case, the potential energy and dipole surfaces were made available to us in the
395 form of a numerical library by Joel Bowman and coworkers.¹² The potential and dipole routines
396 take a single coordinate vector as input and return the respective energy value or 3-component
397 dipole vector.

398 The Heidelberg MCTDH implementation^{42,47,59-62} relies on an explicit numerical represen-
399 tation of the potential in terms of a sum of products of one- or low-dimensional functions which
400 are sampled on a primitive grid. Hence, given a numerical library routine for the potential (and
401 dipoles), a preprocessing step is necessary that creates the required numerical representation of
402 the potential from the output of the library routines.

403 In the present case the potential energy surface has been decomposed into a sum-of-products
404 of 2048 low-dimensional terms, more precisely into a Canonical Polyadic Decomposition form.
405 The low-dimensional basis functions are defined on the coordinates that correspond to those of
406 the bottom layer of the wavefunction tree, (cf. Fig. S10, extended data). Such a decomposition
407 can be used within the Heidelberg MCTDH package. The decomposition was created using a
408 Monte-Carlo variant¹⁸ of the alternating least squares algorithm that is often employed to obtain
409 canonical decompositions. In total eight symmetries have been incorporated into the PES fit,
410 all of them with respect of rotations of the outer water ligands. Other symmetries could not be

411 implemented due to mixing of coordinates. For details about the algorithm the reader is referred
412 to Ref. 18.

413 The surface fit needs to be performed in the internal dynamical coordinates, the library
414 routines usually require Cartesian coordinates to calculate the respective potential energy such
415 that here we interlinked the TANA program with fitting program to be able to transform between
416 the two sets of coordinates.

417 **Data availability**

418 The raw data for Figures 1, 2 and 4 as well as all necessary input files and instructions compat-
419 ible with the Heidelberg MCTDH package are provided to reproduce the infrared spectrum of
420 the Eigen cation. These data are accessible under the URL [https://doi.org/10.5281/
421 zenodo.7064870](https://doi.org/10.5281/zenodo.7064870).

422 **Code availability**

423 The TANA and MCTDH codes with their full documentation and any further input files needed
424 to reproduce particular results of the current contribution are available upon request from the
425 authors.

426 **References**

427 [1] Marx, D., Tuckerman, M., Hutter, J. & Parrinello, M. The nature of the hydrated excess
428 proton in water. *Nature* **397**, 601–604 (1999).

429 [2] Vendrell, O., Gatti, F. & Meyer, H.-D. Dynamics and infrared spectroscopy of the proto-
430 nated water dimer. *Angew. Chem. Int. Ed.* **46**, 6918–6921 (2007).

- 431 [3] Hammer, N. I. *et al.* The vibrational predissociation spectra of the $\text{H}_5\text{O}_2^+ \cdot \text{RG}_n$
432 (RG=Ar,Ne) clusters: Correlation of solvent perturbations in the free OH and shared pro-
433 ton transitions of the Zundel ion. *J. Chem. Phys.* **122**, 244301 (2005).
- 434 [4] Huang, X., Braams, B. J. & Bowman, J. M. *Ab initio* potential energy and dipole moment
435 surfaces for H_5O_2^+ . *J. Chem. Phys.* **122**, 044308 (2005).
- 436 [5] Vendrell, O., Gatti, F., Lauvergnat, D. & Meyer, H.-D. Full dimensional (15D) quantum-
437 dynamical simulation of the protonated water dimer I: Hamiltonian setup and analysis of
438 the ground vibrational state. *J. Chem. Phys.* **127**, 184302 (2007).
- 439 [6] Vendrell, O., Gatti, F. & Meyer, H.-D. Full dimensional (15D) quantum-dynamical sim-
440 ulation of the protonated water dimer II: Infrared spectrum and vibrational dynamics.
441 *J. Chem. Phys.* **127**, 184303 (2007).
- 442 [7] Vendrell, O. & Meyer, H.-D. A proton between two waters: insight from full-dimensional
443 quantum-dynamics simulations of the $[\text{H}_2\text{O}-\text{H}-\text{OH}_2]^+$ cluster. *Phys. Chem. Chem. Phys.*
444 **10**, 4692–4703 (2008).
- 445 [8] Vendrell, O., Gatti, F. & Meyer, H.-D. Strong isotope effects in the infrared spectrum of
446 the zundel cation. *Angew. Chem. Int. Ed.* **48**, 352 – 355 (2009).
- 447 [9] Wolke, C. T. *et al.* Spectroscopic snapshots of the proton-transfer mechanism in water.
448 *Science* **354**, 1131 (2016).
- 449 [10] Yu, Q. & Bowman, J. M. High-level quantum calculations of the ir spectra of the eigen,
450 zundel and ring isomers of $\text{h}^+(\text{h}_2\text{o})_4$ find a single match to experiment. *J. Am. Chem. Soc.*
451 **139**, 10984 (2017).

- 452 [11] Duong, C. H. *et al.* Tag-Free and Isotopomer-Selective Vibrational Spectroscopy of the
453 Cryogenically Cooled H_9O_4^+ Cation with Two-Color. IR-IR Double Resonance Photoex-
454 citation: Isolating the Spectral Signature of a single OH Group in the hydronium Ion Core.
455 *J. Phys. Chem. A* **122**, 9275 (2018).
- 456 [12] Yu, Q. & Bowman, J. M. Communication: Vscf/vci vibrational spectroscopy of h_7o_3^+ and
457 h_9o_4^+ using high-level, many-body potential energy surface and dipole moment surfaces.
458 *J. Chem. Phys.* **146**, 121102 (2017).
- 459 [13] Esser, T. K. *et al.* Deconstructing Prominent Bands in the Terahertz Spectra of H_7O_3^+ and
460 H_9O_4^+ : Intermolecular Modes in Eigen Clusters. *Phys. Chem. Lett.* **9**, 798 (2018).
- 461 [14] Yu, Q. & Bowman, J. M. Classical, thermostated ring polymer, and quantum vscf/vci
462 calculations of ir spectra of h_7o_3^+ and h_9o_4^+ (eigen) and comparison with experiment. *J.*
463 *Phys. Chem. A* **123**, 1399 (2019).
- 464 [15] Yu, Q. & Bowman, J. M. Tracking Hydronium/Water Stretches in Magic $\text{H}_3\text{O}^+(\text{H}_2\text{O})_{20}$
465 Clusters through High-level Quantum VSCF/VCI Calculations. *J. Phys. Chem. A* **124**,
466 1167 (2020).
- 467 [16] Duong, C. H. *et al.* Disentangling the complex vibrational spectrum of the protonated wa-
468 ter trimer, H_7O_3^+ , with two-color IR-IR photodissociation of the bare ion and anharmonic
469 VSCF/VCI theory. *J. Chem. Phys. Lett.* **8**, 3782 (2017).
- 470 [17] Ndong, M. *et al.* Automatic computer procedure for generating exact and analytical kinetic
471 energy operators based on the polyspherical approach: general formulation and removal
472 of singularities. *J. Chem. Phys.* **139**, 204107 (2013).
- 473 [18] Schröder, M. Transforming high-dimensional potential energy surfaces into a canonical
474 polyadic decomposition using Monte Carlo methods. *J. Chem. Phys.* **152**, 024108 (2020).

- 475 [19] Wang, H. & Thoss, M. Multilayer formulation of the multiconfiguration time-dependent
476 Hartree theory. *J. Chem. Phys.* **119**, 1289–1299 (2003).
- 477 [20] Manthe, U. A multilayer multiconfigurational time-dependent Hartree approach for quan-
478 tum dynamics on general potential energy surfaces. *J. Chem. Phys.* **128**, 164116 (2008).
- 479 [21] Vendrell, O. & Meyer, H.-D. Multilayer multiconfiguration time-dependent Hartree
480 method: Implementation and applications to a Henon-Heiles Hamiltonian and to pyrazine.
481 *J. Chem. Phys.* **134**, 044135 (2011).
- 482 [22] Meyer, H.-D., Le Quéré, F., Léonard, C. & Gatti, F. Calculation and selective popula-
483 tion of vibrational levels with the Multiconfiguration Time-Dependent Hartree (MCTDH)
484 algorithm. *Chem. Phys.* **329**, 179–192 (2006).
- 485 [23] Doriol, L. J., Gatti, F., Iung, C. & Meyer, H.-D. Computation of vibrational energy lev-
486 els and eigenstates of fluoroform using the multiconfiguration time-dependent Hartree
487 method. *J. Chem. Phys.* **129**, 224109 (2008).
- 488 [24] Fournier, J. A. *et al.* Snapshots of Proton Accommodation at a Microscopic Water Surface:
489 Understanding the Vibrational Spectral Signatures of the Charge Defect in Cryogenically
490 Cooled H(+)(H₂O)_(n=2-28) Clusters. *J. Phys. Chem. A* **119**, 9425 (2015).
- 491 [25] Yu, Q. & Bowman, J. M. How the Zundel (H₅O₂⁺) Potential Can Be Used to Pre-
492 dict the Proton Stretch and Bend Frequencies of Larger Protonated Water Clusters.
493 *J. Chem. Phys. Lett.* **7**, 5259 (2016).
- 494 [26] Heindel, J., Yu, Q., Bowman, J. & Xantheas, S. Benchmark Electronic Structure Calcu-
495 lations for H₃O⁺(H₂O)_n, n = 0–5 Clusters and Tests of an Existing 1,2,3-body Potential
496 Energy Surface with a New 4-body Correction. *J. Chem. Theory Comput.* **14**, 4553 (2018).

- 497 [27] Yu, Q., Carpenter, W. B., Lewis, N. H. C., Tokmakoff, A. & Bowman, J. M. High-
498 Level VSCF/VCI Calculations Decode the Vibrational Spectrum of the Aqueous Proton.
499 *J. Phys. Chem. B* **123**, 7214 (2019).
- 500 [28] M, A. B. *et al.* Beyond Badger's Rule: The Origins and Generality of the Struc-
501 ture-Spectra Relationship of Aqueous Hydrogen Bonds. *J. Chem. Phys. Lett.* **10**, 918
502 (2019).
- 503 [29] Vendrell, O., Brill, M., Gatti, F., Lauvergnat, D. & Meyer, H.-D. Full dimensional (15D)
504 quantum-dynamical simulation of the protonated water dimer III: mixed Jacobi-valence
505 parametrization and benchmark results for the zero-point energy, vibrationally excited
506 states and infrared spectrum. *J. Chem. Phys.* **130**, 234305 (2009).
- 507 [30] Vendrell, O., Gatti, F. & Meyer, H.-D. Full dimensional (15D) quantum-dynamical simu-
508 lation of the protonated water dimer IV: Isotope effects in the infrared spectra of $D(D_2O)_2^+$,
509 $H(D_2O)_2^+$ and $D(H_2O)_2^+$ isotopologues. *J. Chem. Phys.* **131**, 034308 (2009).
- 510 [31] Markovitch, O. *et al.* Special Pair Dance and Partner Selection: Elementary Steps in
511 Proton Transport in Liquid Water. *J. Phys. Chem. B* **112**, 9456–9466 (2008). URL
512 <https://doi.org/10.1021/jp804018y>.
- 513 [32] Kulig, W. & Agmon, N. A 'clusters-in-liquid' method for calculating infrared spec-
514 tra identifies the proton-transfer mode in acidic aqueous solutions. *Nat. Chem.* **5**, 29–
515 35 (2013). URL <http://www.nature.com/nchem/journal/v5/n1/full/nchem.1503.html>.
516
- 517 [33] Calio, P. B., Li, C. & Voth, G. A. Resolving the structural debate for the hydrated excess
518 proton in water. *J. Am. Chem. Soc.* **143**, 18672 (2021).

- 519 [34] Fournier, J. A., Carpenter, W. B., Lewis, N. H. C. & Broadband, A. 2d ir spectroscopy
520 reveals dominant asymmetric H_5O_2^+ proton hydration structures in acid solutions. *Nat.*
521 *Chem.* **10**, 932–937 (2018).
- 522 [35] Carpenter, W. B., Fournier, J. A., Lewis, N. H. C. & Tokmakoff, A. Picosecond proton
523 transfer kinetics in water revealed with ultrafast ir spectroscopy. *J. Phys. Chem. B* **122**,
524 2792–2802 (2018).
- 525 [36] Kundu, A. *et al.* Hydrated excess protons in acetonitrile/water mixtures: Solvation species
526 and ultrafast proton motions. *J. Phys. Chem. Lett.* **10**, 2287–2294 (2019).
- 527 [37] Gatti, F. *et al.* Vector parametrization of the n-atom problem in quantum mechanics. I.
528 Jacobi vectors. *J. Chem. Phys.* **108**, 8804 (1998).
- 529 [38] Gatti, F. Vector parametrization of the n-atom problem in quantum mechanics. III. Sepa-
530 ration into two sub-systems. *J. Chem. Phys.* **111**, 7225 (1999).
- 531 [39] Gatti, F. & Iung, C. Exact and constrained kinetic energy operators for polyatomic
532 molecules: The polyspherical approach. *Phys. Rep.* **484**, 1–69 (2009).
- 533 [40] Ndong, M. *et al.* Automatic computer procedure for generating exact and analytical kinetic
534 energy operators based on the polyspherical approach. *J. Chem. Phys.* **136**, 034107 (2012).
- 535 [41] Lauvergnat, D. TNUM-TANA: A fortran code for coordinate transformations and kinetic
536 energy operators. See <https://github.com/lauvergn/EIVibRot-TnumTana>.
- 537 [42] Meyer, H.-D. Studying molecular quantum dynamics with the multiconfiguration time-
538 dependent Hartree method. *WIREs: Comput. Mol. Sci.* **2**, 351–374 (2012). URL <http://dx.doi.org/10.1002/wcms.87>.
539

- 540 [43] Wang, H. Multilayer Multiconfiguration Time-Dependent Hartree Theory. *J. Phys.*
541 *Chem. A* **119**, 7951 (2015).
- 542 [44] Tucker, L. Some mathematical notes on three-mode factor-analysis. *Psychometrika* **31**,
543 279 (1966).
- 544 [45] Hackbusch, W. & Kühn, S. A new scheme for the tensor representation. *Journal of Fourier*
545 *Analysis and Applications* **15**, 706–722 (2009).
- 546 [46] Grasedyck, L. & Hackbusch, W. An Introduction to Hierarchical (\mathcal{H} -) Rank and TT-Rank
547 of Tensors with Examples. *Comp.Meth.Appl.Math* **11**, 291–304 (2011).
- 548 [47] Beck, M. H., Jäckle, A., Worth, G. A. & Meyer, H.-D. The multi-configuration time-
549 dependent Hartree (MCTDH) method: A highly efficient algorithm for propagating wave
550 packets. *Phys. Rep* **324**, 1–105 (2000).
- 551 [48] Jäckle, A. & Meyer, H.-D. Product representation of potential energy surfaces. *J. Chem.*
552 *Phys.* **104**, 7974 (1996).
- 553 [49] Jäckle, A. & Meyer, H.-D. Product representation of potential energy surfaces II. *J. Chem.*
554 *Phys.* **109**, 3772 (1998).
- 555 [50] Otto, F. Multi-Layer Potfit: An accurate potential representation for efficient high-
556 dimensional quantum dynamics. *J. Chem. Phys.* **140**, 014106 (2014).
- 557 [51] Peláez, D. & Meyer, H.-D. The multigrid POTFIT (MGPF) method: Grid representations
558 of potentials for quantum dynamics of large systems. *J. Chem. Phys.* **138**, 014108 (2013).
- 559 [52] Schröder, M. & Meyer, H.-D. Transforming high-dimensional potential energy surfaces
560 into sum-of-products form using Monte Carlo methods. *J. Chem. Phys.* **147**, 064105
561 (2017).

- 562 [53] Otto, F., Chiang, Y.-C. & Peláez, D. Accuracy of Potfit-based potential representations
563 and its impact on the performance of (ML-)MCTDH. *Chem. Phys.* **509**, 116 (2018).
- 564 [54] Hitchcock, F. L. The expression of a tensor or a polyadic as a sum of products. *J. Math.*
565 *Phys.* **6**, 164–189 (1927).
- 566 [55] Harshman, R. A. Foundations of the PARAFAC procedure: Models and conditions for
567 an "explanatory" multi-modal factor analysis. *UCLA Working Papers in Phonetics* **16**, 1
568 (1970).
- 569 [56] Carroll, J. D. & Chang, J.-J. Analysis of individual differences in multidimensional scaling
570 via an n-way generalization of "Eckart-Young" decomposition. *Psychometrika* **35**, 283
571 (1970).
- 572 [57] Gatti, F. & Meyer, H.-D. Intramolecular vibrational energy redistribution in Toluene: A
573 nine dimensional quantum mechanical study using the MCTDH algorithm. *Chem. Phys.*
574 **304**, 3–15 (2004).
- 575 [58] Lauvergnat, D. & Nauts, A. Exact numerical computation of a kinetic energy operator in
576 curvilinear coordinates. *J. Chem. Phys.* **116**, 8560 (2002).
- 577 [59] Meyer, H.-D., Manthe, U. & Cederbaum, L. S. The multi-configurational time-dependent
578 Hartree approach. *Chem. Phys. Lett.* **165**, 73–78 (1990).
- 579 [60] Manthe, U., Meyer, H.-D. & Cederbaum, L. S. Wave-packet dynamics within the mul-
580 ti-configuration Hartree framework: General aspects and application to NOCl. *J. Chem.*
581 *Phys.* **97**, 3199–3213 (1992).

582 [61] Meyer, H.-D. & Worth, G. A. Quantum molecular dynamics: Propagating wavepack-
583 ets and density operators using the multiconfiguration time-dependent Hartree (MCTDH)
584 method. *Theor. Chem. Acc.* **109**, 251–267 (2003).

585 [62] Meyer, H.-D., Gatti, F. & Worth, G. A. (eds.) *Multidimensional Quantum Dynamics:*
586 *MCTDH Theory and Applications* (Wiley-VCH, Weinheim, 2009).

587 **Acknowledgments**

588 The authors thank Prof. Mark Johnson and Prof. Knut Asmis for sharing experimental data
589 with us and Prof. Joel Bowman for the source code of the potential energy surface. We fur-
590 thermore thank the High Performance Computing Center in Stuttgart (HLRS) under the grant
591 number HDQM_MCT as well as the bwHPC project of the state of Baden-Württemberg under
592 grant number bw18K011 for providing computational resources. The authors thank the CNRS
593 International Research Network (IRN) "MCTDH" for financial support.

594 **Author contributions**

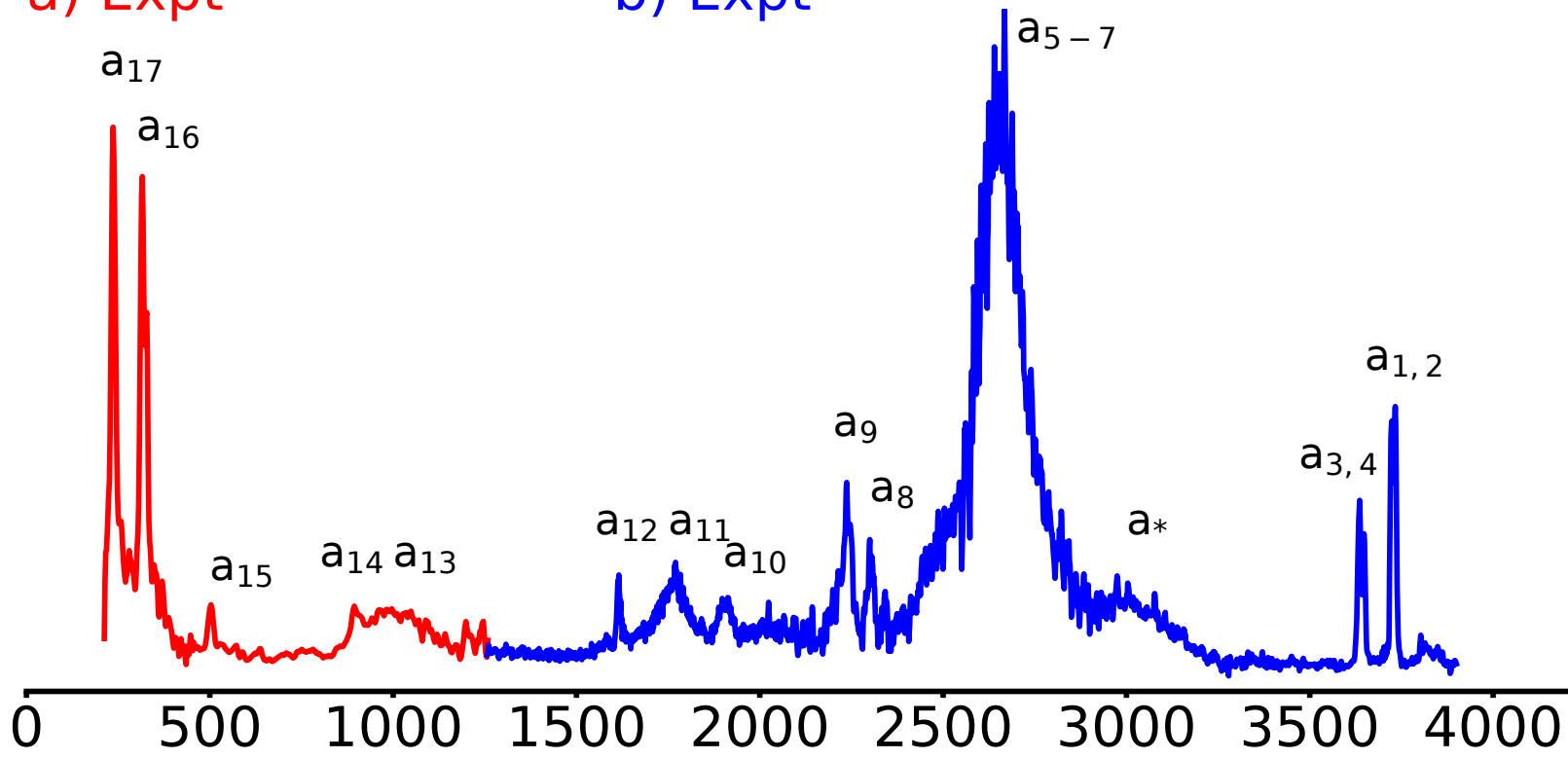
595 M.S., H.-D.M. and O.V. conceived the idea and planed the calculations and the analysis method-
596 ology. M.S. contributed the SOP fitting of the PES and DMS and performed the dynamical
597 calculations and analysis. F.G., D.L. and O.V. designed the coordinates system. F.G. and D.L.
598 generated the corresponding analytical KEO. The text was initially composed by M.S. and O.V.,
599 and all authors contributed to the discussion and interpretation of the results and to the final ver-
600 sion of the manuscript.

601 **Competing interests**

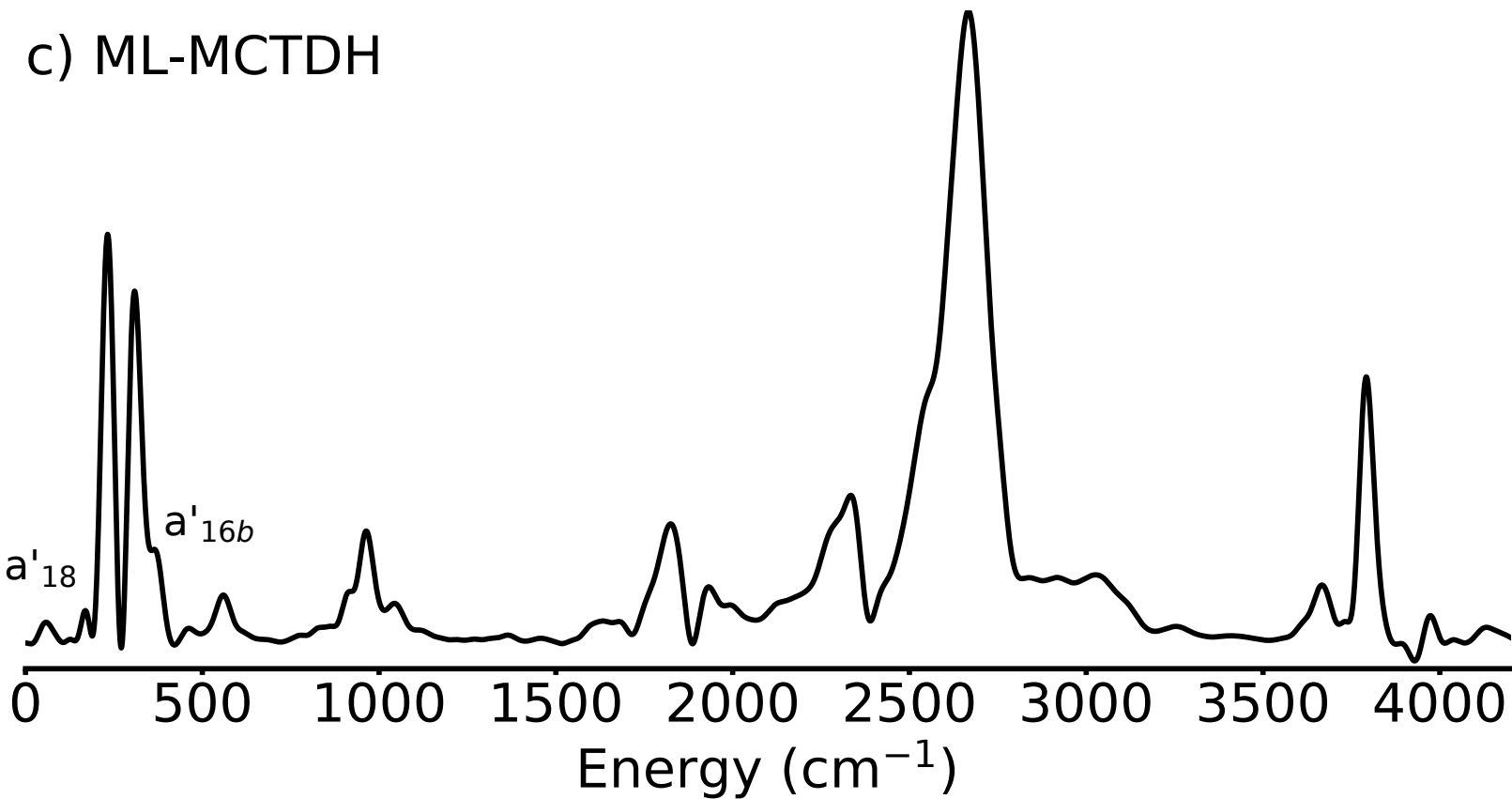
602 The authors have no competing interests.

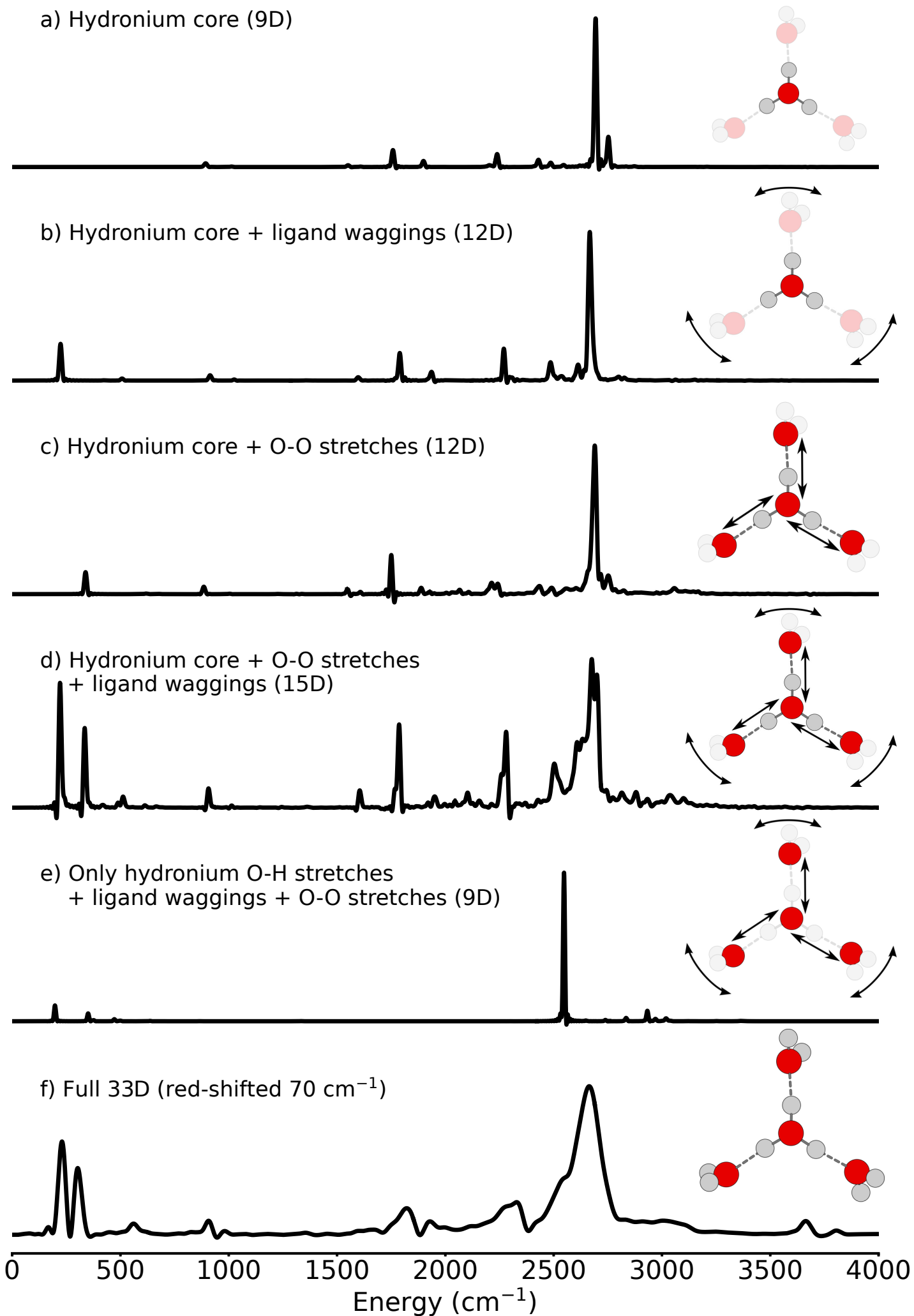
a) Expt

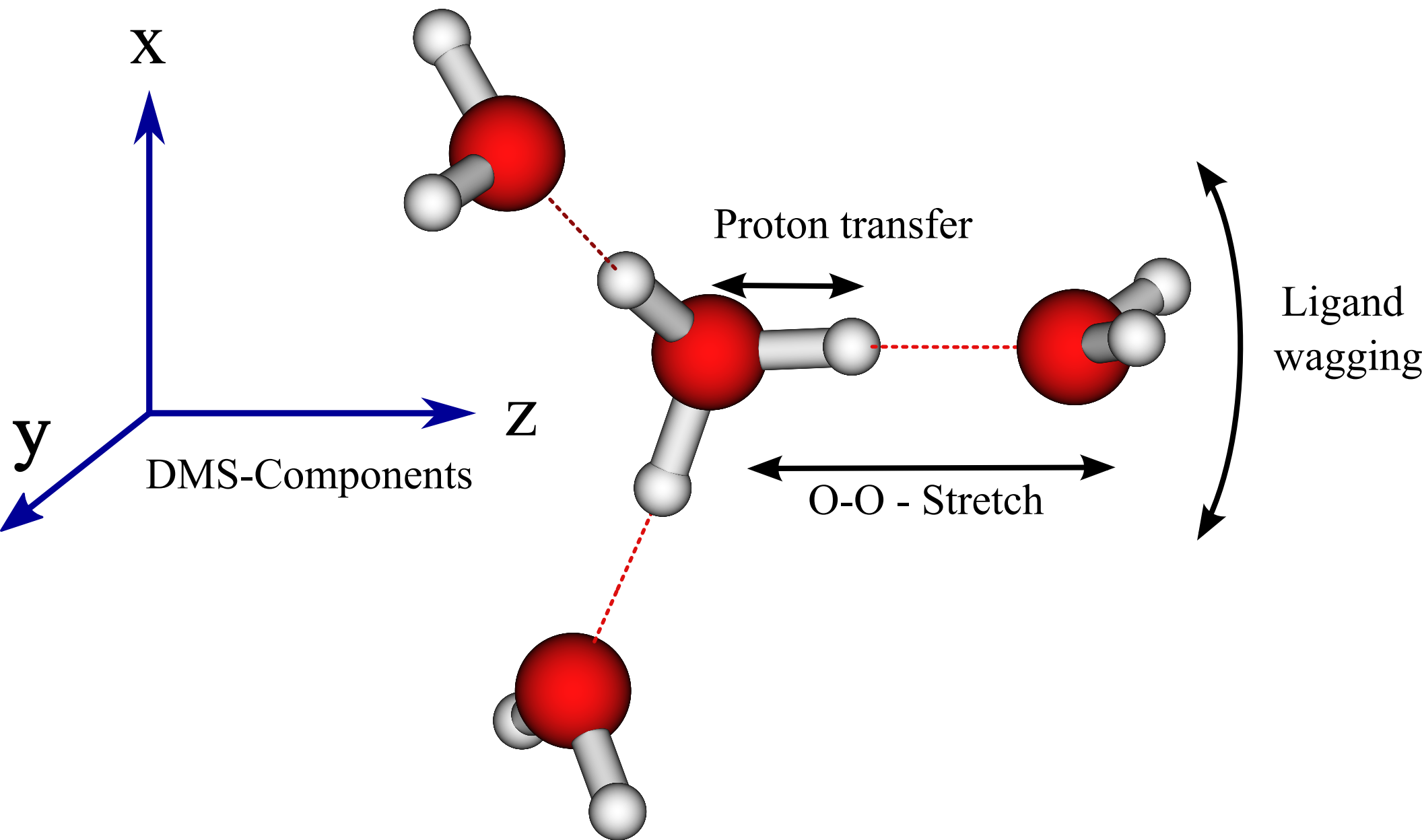
b) Expt



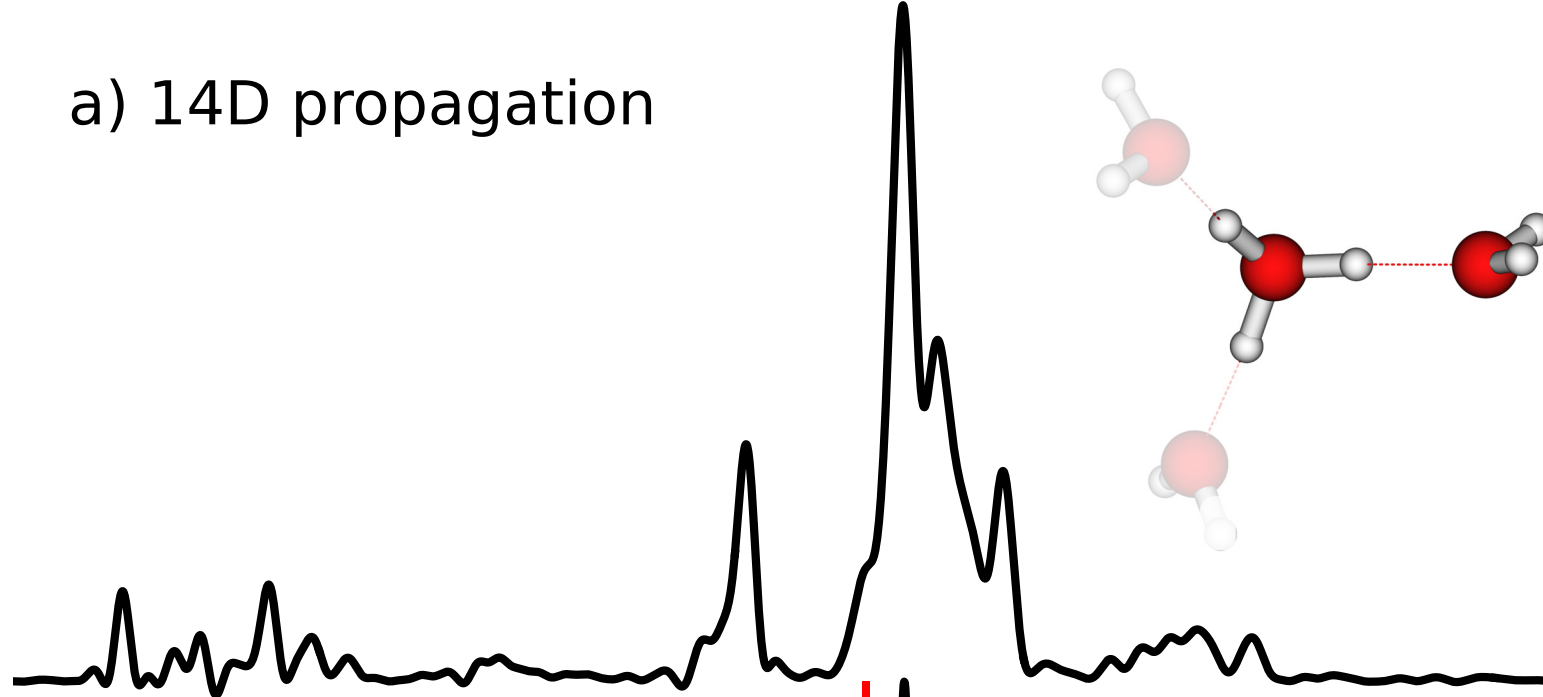
c) ML-MCTDH







a) 14D propagation



b) 9D propagation
and stick

